RSC Advances

COMMUNICATION

View Article Online
View Journal | View Issue

Cite this: *RSC Adv.*, 2015, **5**, 38842

Gold nanorod encapsulated bubbles†

A. Tomak[a] and H. M. Zareie*[ab]

Received 20th February 2015
Accepted 17th April 2015

DOI: 10.1039/c5ra03240g

www.rsc.org/advances

A simple method has been described for synthesizing gold nanorods (GNRs) encapsulated bubbles in a controlled manner. The method involves the use of nitrogen gas in the seed-mediated synthesis method routinely used for synthesis of GNRs. Control over the morphology of the nanostructures was achieved by nitrogen gas flow. The synthesized structures were examined by UV-Vis Spectroscopy, Scanning Electron Microscopy (SEM) and Atomic Force Microscopy (AFM). New structures of this type could conceivably serve as plasmonic biosensors, nanodevices and photothermal theranostics with dual modality imaging functionality.

The shape of gold nanoparticles (GNPs) plays a significant role in their functions, since electronic, magnetic and optical properties of GNPs depend not only on the size, but also on the shape of the particles.[1–3] There is an extensive number of studies in the literature for the synthesis of gold nanocrystals with various forms including nanorods,[4–6] nanoshells,[7,8] nanorattles[9] and hollow structures (cages and boxes).[10,11] Gold nanorods (GNRs) with peculiar optical properties have become a favorite for a variety of applications such as optical devices, imaging and therapy.[9,12,13] Seed-mediated synthesis in aqueous solution is a typical process for GNR production. Varying approaches and chemicals have been used in this process for synthesizing GNRs.[14–16] Uniformly shaped rods with controlled and high aspect ratio (4.6, 13 and 18) were formed in an aqueous micellar template *via* a seeding growth method varying the ratio of seed to metal salt.[17] The hydrocarbon chain length of the surfactant molecules used in GNRs synthesis was found to have a critical effect on the aspect ratio, longer chain lengths yielding longer GNRs.[18] The changes in the environment of GNRs during or after the synthesis or conjugation with other molecules may introduce new nanocrystal forms with various shapes and sizes. For example, increasing solution temperature reduced the length and hence the mean aspect ratio of GNRs having an aspect ratio higher than 2.[19] Threadlike gold nanostructures have been formed *via* photochemical reduction in the presence of cetyltrimethylammonium chloride.[20] Synthesis of more complex structures such as nanorattles with gold particle cores and Pt/Ag shells, and nanorattles of gold nanorods and hollow gold nanocrystallines with solid nanorods inside has recently been reported.[9,21] However, to the best of our knowledge, no group has yet suggested a method to directly synthesize GNRs embedded nanobubbles which are nanostructures potentially useful for various applications including bioimaging and photothermal therapy. Herein, we describe a simple method introducing an inert gas flow to seed solution utilized in commonly used seed-mediated GNR synthesis. Introduction of an inert gas during GNR synthesis leads to the formation of nanobubbles encapsulating multiple GNRs. We further demonstrate the photothermal effect of gold nanobubbles (GNBs).

A well-defined method described by Smith *et al.*[1] for synthesis of GNRs *via* seed-mediated growth was adapted for synthesis of GNBs. Nitrogen (N_2) or argon (Ar) was used as an inert gas. The gas flow was supplied using a pressurized cylinder with a controllable pressure gauge. First, N_2 gas flow at 200–250 sccm was applied only to seed solution during GNR synthesis. While a negligible amount of nanorods formed in solution, the main structures dominantly observed were nanobubbles encapsulating a number of GNRs (Fig. 1A–C). The bubble periphery under low keV electron beam of SEM appeared to have a dense structure. However, as soon as the bubbles were exposed to a higher keV (5–10 keV) electron beam, the bubbles became transparent (Fig. S1†), suggesting that the periphery of nanobubbles was composed of hexadecyltrimethylammonium bromide (CTAB) present in seed and growth solutions.

[a]*Department of Material Science and Engineering, Izmir Institute of Technology, Urla, Izmir, 35430, Turkey. E-mail: hadizareie@iyte.edu.tr*

[b]*Microstructural Analysis Unit, School of Physics and Advanced Materials, University of Technology, Ultimo, Sydney, NSW 2007, Australia*

† Electronic supplementary information (ESI) available: Materials and experimental methods, SEM micrographs of GNP synthesis under Ar, Raman spectroscopy of bubbles, UV-Vis spectroscopy results of GNP synthesis under Ar gas and photothermal effect of new GNB structure. See DOI: 10.1039/c5ra03240g

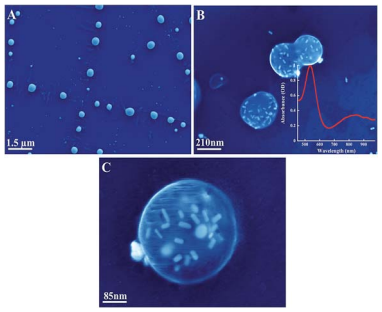

Fig. 1 SEM images of nanobubbles. (A) Large area image (B) magnified region from image A. (inset: UV-Vis spectrum of nanobubbles). (C) High magnification image of nanobubbles.

The UV-Vis spectrum of nanobubble solution showed shorter wavelength absorption peak at 520 nm, indicative of plasmon oscillations in the shorter transverse direction, together with a weak longer wavelength peak at 800 nm, attributable to longitudinal oscillations of electrons in GNRs encapsulated in the bubble structure (Fig. 1B-inset). The strength of the longitudinal surface plasmon resonance peak (at 800 nm) is smaller than that of the transverse direction oscillation peak at 520 nm. This may due to the presence of the dense CTAB layer around the bubbles containing nanorods, decreasing the intensity of absorption at 800 nm. Overall the UV-Vis measurement verified the presence of GNRs in the nanobubbles. The SEM images (Fig. 1A–C) demonstrated the presence of bubbles with diameters ranging between 200 and 600 nm.

The existence of nitrogen gas in the bubbles was confirmed using Raman spectroscopy (Fig. S2A and B†). The Raman analysis of water without bubbles after purging with Ar gas showed that the band at 2329 cm^{-1}, which is characteristic to N_2 gas, completely disappeared. This indicated the removal of N_2 gas dissolved in water upon purging with Ar gas. At the next step, Ar gas was introduced into the bubble solution and the solution was analyzed by Raman spectroscopy. In this case, N_2 gas band at 2329 cm^{-1} along with the bands characteristic to CTAB molecules (CH_3's 2 asymmetric and 2 symmetric peaks at 1453, 2926, 2848 and 2886 cm^{-1}) were clearly observed, evidencing that the bubbles contained N_2 gas. In conclusion, the results indicated that the nanostructures were indeed bubbles and not micelles.

Next, a series of control experiments were performed to understand the effect of N_2 gas flow on the formation of new nanostructures, GNRs encapsulated nanobubbles. When the gas flow was applied to both seed and growth solutions, or growth solution only, GNRs were observed without any bubble formation. This indicated that N_2 flow is needed only in the seed solution for the formation of nanobubbles. It can be speculated that during seed formation some CTAB molecules surround gas bubbles through hydrophobic interactions and seed particles are embedded in the wall of the CTAB stabilized gas bubbles. Upon addition of growth solution, CTAB micelles complexed with $AuCl_2^-$ ions collide with CTAB stabilized bubbles embedded with seed particles. Thus $AuCl_2^-$ ions from

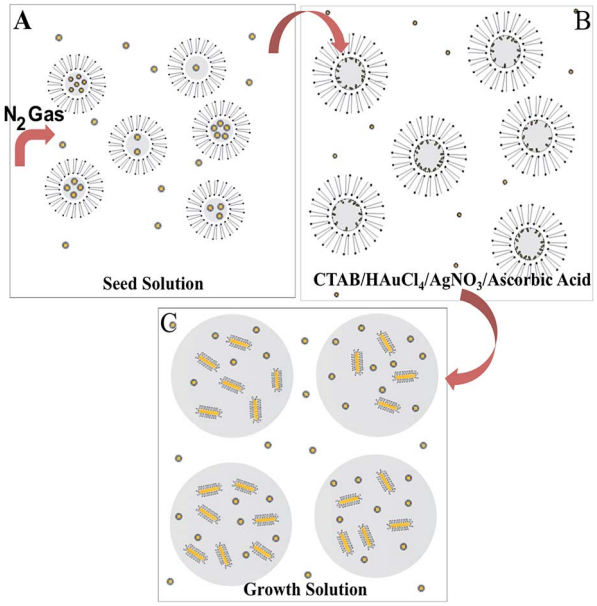

Scheme 1 Schematic illustration of the synthesis process of gold nanorod embedded bubbles.

growth solution interact with seed particles at the interface of the bubble and solution resulting in inward longitudinal growth of seed particles to GNRs in the wall of bubbles (Scheme 1). GNR growth might be limited by the time point at which the nanorods are too large to stay stably attached to the bubble–solution interface. Indeed, the low keV SEM images of GNBs at high magnification clearly revealed the presence of nanorods embedded in the wall of GNBs (Fig. S3†).

Application of gas flow into both seed and growth solutions resulted in formation of GNRs only without bubble formation. This may be explained by possible destabilization and mechanically disruption of CTAB-stabilized gas bubbles in seed solution by gas flow run through growth solution during addition of seed solution.

The effect of inert gas type on GNB synthesis was also investigated by replacing N_2 with Ar. Fig. S4† shows the SEM micrograph of the resultant structures obtained when Ar gas flow was applied at a rate of 200–250 sccm into seed solution during GNR synthesis. The SEM results indicated that no bubbles were formed. GNPs along with GNRs were observed on SEM micrographs. This result was attributed to the lower solubility of Ar in aqueous solution when compared with N_2, which results in reduced interactions of gas bubbles with CTAB molecules in solution.

The effect of gas flow rate on GNB formation was also investigated for both of gases utilized. No effect on particle formation was observed in the studied range (200–250 sccm).

The stability of GNBs in water was followed for up to 6 months. The bubbles were found to keep their structural integrity for 5 months, as observed by SEM. After 6 months, the integrity of the bubbles was lost (Fig. S5A and B†).

Next we applied the same approach to the seedless synthesis method of GNRs described by Jana *et al.*[22] Fig. 2A displays the

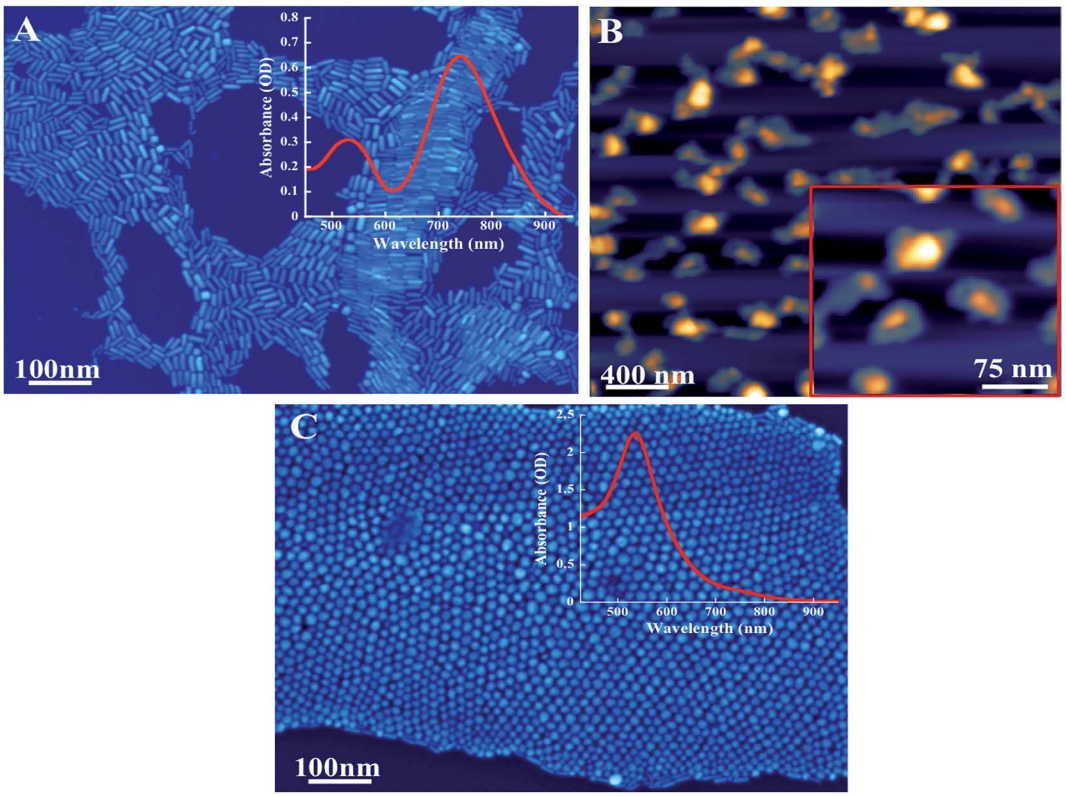

Fig. 2 (A and C) SEM micrograph of GNRs and GNPs (insets: UV-Vis spectra of GNRs and GNPs). (B) AFM images of GNRs (inset: high magnification image obtained using AFM).

SEM micrograph and UV-Vis spectrum of the resultant solution obtained in the absence of gas flow. As expected GNRs were produced *via* the well-known seedless synthesis method. From the SEM micrograph, the size of GNRs was determined to be 10 nm in diameter and 30 nm in longitude. The UV-Vis spectrum (inset in the same figure) shows typical two peaks for GNRs. The first peak at 530 nm indicates the transverse plasmon band and the second peak shows a strong absorption band at 750 nm due to longitudinal oscillations of electrons. The AFM micrographs show the size of GNRs to be 20 nm in diameter and 80 nm in length (Fig. 2B). These sizes were larger than the ones calculated from SEM micrographs due to broadening effect of the AFM tip and the CTAB layer surrounding the nanorods that can be clearly observed in the AFM micrograph.

Fig. 2C shows the SEM micrograph of the final product obtained in the presence of N_2 flow at a rate of 200–250 sccm. When the gas flow was applied, only GNPs were observed to form instead of GNRs or nanobubbles encapsulating GNRs. It is possible that the gas bubbles inside the solution were surrounded by CTAB molecules through hydrophobic interactions. In other words, the gas bubbles act as CTAB traps, preventing the formation of stabilized CTAB bilayers around nanoparticles required for the longitudinal growth of seed particles to GNRs (Scheme 1). Fig. 2C (inset) illustrates the UV-Vis spectrum of the particles obtained in the presence of N_2 gas flow. A single short-wavelength peak observed at 530 nm, which is typical for nanoparticle formation. Although the presence of an insignificant amount of nanorods was observable in the SEM micrograph, it appeared to be negligible to have optical response as verified by the absence of a second peak indicative of GNRs in the UV-Vis spectrum.

The effect of inert gas type was also investigated by replacing N_2 with Ar. Fig. S6† shows the SEM micrograph and UV-Vis spectrum of the final structures obtained when Ar gas flow was applied at a rate of 200–250 sccm into seedless synthesis solution. The spectrum clearly showed the formation of GNPs. The λ_{max} of the absorption peak in the UV-Vis spectrum was at 530 nm that is typical for the particles. However, the shape of the particles was different than spherical particles obtained using N_2 gas. Most of the GNPs formed under Ar flow had octahedral shapes. This suggested certain degree of longitudinal growth which did not complete with the formation of a full rod shape, possibly caused by reduced interactions of Ar bubbles with CTAB molecules in solution due to lower solubility of Ar.

The effect of gas flow rate on particle formation using seedless synthesis method was also investigated. No effect on particle formation was observed in the studied range (50–150) sccm.

Finally, photothermal effect of new GNB structure was investigated considering the potential use of these structures in photothermal therapy. An 808 nm diode laser was used to heat the gold nanobubble solution. The temperature of nanobubble solution at a fixed concentration (15.2 mg L^{-1}) was observed to increase from 20 °C to 36.3 °C and 38.6 °C in 10 and 20 minutes, respectively, under laser irradiation, indicating the efficient

photothermal effect of new nanobubble structures. The temperature rise in nanobubble solution was also monitored using a thermal camera after 20 minutes of laser irradiation. As it is seen in the picture, there is a temperature gradient across the *x*-axis of the tube containing solution. The center has the highest temperature around 40 °C and the sides around 36 °C (Fig. S7†). The photothermal effect of nanorods alone was also investigated for comparison purpose. The temperature of the nanorod solution at a fixed concentration increased from 20 °C to 45 °C in 20 minutes under laser irradiation. The decreased photothermal effect in the case of nanobubbles might be due to the presence of the CTAB shell and N_2 gas in the bubbles. Hence in terms of photothermal effect only, the nanobubble structure showed no direct advantage over the nanorods alone.

Conclusions

We report a simple method for direct synthesis of nanobubbles encapsulating gold nanorods. The method utilizes the seed-mediated synthesis well-established for preparation of gold nanorods. It involves the use of N_2 gas flow during seed preparation. The new nanostructures produced by this method are simply N_2 gas bubbles surrounded by surfactant molecules. The bubbles, having an average diameter of 200–600 nm, contain a number of gold nanorods inside. These new structures display photothermal effect as expected.

One can envisage the use of the gold nanorods embedded bubble structures in the field of theranostics. These structures have several features that potentially make them improved theranostics. These features potentially include (i) photothermal effect, (ii) capacity to carry chemotherapeutics in the wall of bubbles, (iii) ability to localize a number of GNRs inside one cell, (iv) photoacoustic/ultrasound dual modality imaging ability. Further work is required to replace CTAB surfactant, a well-known toxic compound, with biocompatible lipid surfactants on the shell of nanobubbles. This design would potentially enable the loading of drug molecules together with GNRs into bubbles, leading to a system with chemo- and photothermal-therapeutic activity and dual modality imaging functionality. It would also be possible to modify the surface of GNBs with biological molecules for active targeting of specific cells and tissues.

Acknowledgements

The authors acknowledge TUBITAK for financial support (PROJECT no. 112T507), Prof. Dr Müjdat Çağlar, Electric and Electronics Department, Anadolu University, Eskisehir, for SEM experiments, and also Reviewer 2 of this manuscript for his/her useful comments on the formation mechanism of GNBs.

Notes and references

1 D. K. Smith and B. A. Korgel, *Langmuir*, 2008, **24**, 644.
2 M. H. Zareie, X. Xu and M. B. Cortie, *Small*, 2007, **3**, 139.
3 C. Burda, X. Chen, R. Narayanan and M. A. El-Sayed, *Chem. Rev.*, 2005, **105**, 1025.
4 X. Ye, C. Zheng, J. Chen, Y. Gao and C. B. Murray, *Nano Lett.*, 2013, **13**, 765.
5 B. Nikoobakht and M. A. El-Sayed, *Chem. Mater.*, 2003, **15**, 1957.
6 B. D. Busbee, S. O. Obare and C. J. Murphy, *Adv. Mater.*, 2003, **15**, 414.
7 T. Pham, J. B. Jackson, N. J. Halas and T. R. Lee, *Langmuir*, 2002, **18**, 4915.
8 A. M. Brito-Silva, R. G. Sobral-Filho, R. Barbosa-Silva, C. B. de Araújo, A. Galembeck and A. G. Brolo, *Langmuir*, 2013, **29**, 4366.
9 Y. Khalavka, J. Becker and C. Sönnichsen, *J. Am. Chem. Soc.*, 2009, **131**, 1871.
10 A. M. Schwartzberg, T. Y. Olson, C. E. Talley and J. Z. Zhang, *J. Phys. Chem. B*, 2006, **110**, 19935.
11 S. E. Skrabalak, J. Chen, Y. Sun, X. Lu, L. Au, C. M. Cobley and Y. Xia, *Acc. Chem. Res.*, 2008, **41**, 1587.
12 I. H. El-Sayed, X. Huang and M. A. El-Sayed, *Nano Lett.*, 2005, **5**, 829.
13 X. Huang, I. H. El-Sayed and M. A. El-Sayed, *Methods in molecular biology*, Clifton, N.J., 2010, vol. 624, p. 343.
14 J. Pérez-Juste, I. Pastoriza-Santos, L. M. Liz-Marzán and P. Mulvaney, *Coord. Chem. Rev.*, 2005, **249**, 1870.
15 J. A. Edgar, A. M. McDonagh and M. B. Cortie, *ACS Nano*, 2012, **6**, 1116.
16 M. A. Mahmoud and M. A. El-Sayed, *J. Phys. Chem. Lett.*, 2013, **4**, 1541.
17 N. R. Jana, L. Gearheart and C. J. Murphy, *J. Phys. Chem. B*, 2001, **105**, 4065.
18 J. Gao, C. M. Bender and C. J. Murphy, *Langmuir*, 2003, **19**, 9065.
19 M. B. Mohamed, K. Z. Ismail, S. Link and M. A. El-Sayed, *J. Phys. Chem. B*, 1998, **102**, 9370.
20 K. Esumi, K. Matsuhisa and K. Torigoe, *Langmuir*, 1995, **11**, 3285.
21 J. Yang, L. Lu, H. Wang and H. Zhang, *Scr. Mater.*, 2006, **54**, 159.
22 N. R. Jana, *Small*, 2005, **1**, 875.